


Mechanism of stacking fault formation in metal(100) heteroepitaxial growth

Indiras Khatri¹,* Ehsan H. Sabbar,[†] Yunsic Shim,[‡] and Jacques G. Amar[§]
Department of Physics & Astronomy, University of Toledo, Toledo, Ohio 43606, USA

 (Received 11 June 2020; accepted 19 October 2020; published 16 November 2020)

Strain in metal(100) heteroepitaxial thin-film growth can lead to a variety of effects such as the formation of stacking faults (SFs). To gain a better understanding we have carried out temperature-accelerated dynamics (TAD) simulations of the submonolayer growth of Cu islands on a biaxially strained Cu substrate at 200 K. In the case of 4% compressive strain we find that SF formation occurs with a morphology very similar to the structures found experimentally in Cu/Ni(100) growth. We also find that islands play a key role by lowering the barrier for vacancy formation. In particular, once two substrate vacancies are formed and diffuse to form the appropriate configuration this leads to the formation of a SF in both the substrate and island. While the activation barrier for SF formation is very high, due to the presence of a large number of low-frequency vibrational modes, the saddle-point entropy is large while the corresponding Vineyard prefactor is more than 10 orders of magnitude larger than is typical of atomic processes in fcc metals. Similarly, an analysis of the entropy of the SF state indicates that the reverse prefactor is much smaller, while the free energy of this state is lower than that of the initial state.

DOI: [10.1103/PhysRevMaterials.4.113403](https://doi.org/10.1103/PhysRevMaterials.4.113403)

I. INTRODUCTION

Strain in heteroepitaxial thin-film growth can lead to a variety of interesting morphological and structural effects [1–18] including dislocation formation [3,11,18] and the Asaro-Tiller-Grinfeld instability [1,2,17], as well as island-shape transitions [4–6,8–10,12,14–16] and stacking faults [6,13]. Of particular interest are the experiments carried out by Müller *et al.* [6–9] in which both submonolayer and multilayer Cu islands grown on a Ni(100) substrate (corresponding to 2.7% compressive strain) were found to form ramified island shapes followed by the subsequent formation of ‘stripe’ defects corresponding to stacking faults.

While it was initially thought [9] that the ramified island shapes might be due to the coalescence of anisotropic (rectangular) islands whose anisotropy was due to strain [5,19], theoretical calculations of the critical island size or armwidth L_c for anisotropy [20] indicate that for Cu/Ni(100), L_c is many orders of magnitude larger than the critical value ($22b$, where b is the nearest-neighbor distance) observed for the formation of ramified islands. Instead, it was found [20] that this corresponds to the critical island size for strain-induced in-plane multiatom ‘pop-out’ events which lead to a competition between open and closed island step edges as is observed experimentally [9].

Kinetic Monte Carlo (KMC) simulations [20] which take these events into account were found to reproduce the

experimentally observed submonolayer island morphologies at 250 K and 300 K. However, since these were on-lattice simulations, they were unable to explain the subsequent formation of stacking faults. We note that stacking faults have been found to play an important role in determining the quality of strained thin films. For example, by blocking the extension of threading dislocations in GaN growth [21], as well as by blocking dislocation motion in ultrahard high-entropy alloy thin films [22], stacking faults have been shown to improve the quality of strained thin films. Accordingly, in order to gain a better understanding of the energetics and kinetics of stacking fault formation as well as to separate out chemical effects from strain effects, we have carried out fully off-lattice temperature-accelerated dynamics (TAD) simulations of the submonolayer growth of Cu islands on a biaxially strained Cu substrate.

In order to maximize the boost due to accelerated dynamics so that we can simulate growth on timescales close to experiments, our simulations were carried out using a relatively low substrate temperature $T = 200$ K. This value also implies that the average island size will be significantly smaller than the typical system size that can be efficiently simulated using TAD [20,23]. In addition, since the substrate temperature was relatively low compared to experiment, our simulations were carried out using a value of the compressive strain (4%) which is somewhat larger than the value (2.7%) for Cu/Ni(100) growth [24].

Somewhat surprisingly, we find that stacking fault formation occurs in our simulations. Our results also indicate that the formation of islands plays a key role in promoting stacking fault formation by lowering the barrier for vacancy formation as well as decreasing the vacancy formation energy. Once two substrate vacancies are formed and diffuse to form the appropriate configuration near an island, this leads to the

*indiras.khatri@rockets.utoledo.edu

[†]Current address: Department of Electrical Engineering, University of Anbar, 11, Ramadi, Iraq; ehsan.sabbar@uoanbar.edu.iq

[‡]yunsic.shim@utoledo.edu

[§]jacques.amar@utoledo.edu

formation of a stacking fault in both the substrate and island, with a morphology very similar to the structures suggested by Müller *et al.* [6,8,9] based on their experiments.

Our results also indicate that while the activation barrier for stacking fault formation is very high (1.0 eV), due to the presence of a large number of low-frequency vibrational modes which increase the saddle-point entropy, the transition rate prefactor is also unusually large ($8.8 \times 10^{27} \text{ s}^{-1}$). As a result, the average time interval for this transition is only 3.2 msec. Similarly, an analysis of the entropy of the stacking fault (SF) state indicates that the reverse prefactor is much smaller and that the free energy of the SF state is lower than that of the initial state. These results indicate that in the presence of compressive strain, the formation of stacking faults is both kinetically and thermodynamically favorable at sufficiently high temperatures.

The organization of this paper is as follows. We first briefly discuss our TAD simulations in Sec. II and then present our results in Sec. III. Finally, in Sec. IV we summarize our results and also discuss the implications for stacking fault formation in Cu/Ni(100) growth.

II. TEMPERATURE-ACCELERATED DYNAMICS SIMULATIONS

In order to access experimental timescales while including both the effects of strain and on-lattice and off-lattice transition pathways, we have carried out temperature-accelerated molecular dynamics (TAD) simulations [23,25–28]. As discussed in more detail in Refs. [23,25–27], TAD simulations are based on the assumption of harmonic transition-state theory along with the use of a molecular dynamics simulation at a high temperature (T_{high}) which is used to accelerate the search for the state-to-state pathways and transition times at a lower temperature (T_{low}). In particular, for each visited state, a high temperature basin-constrained MD simulation is first carried out to determine the possible escape pathways along with the corresponding high-temperature transition times and activation barriers. Once sufficient information has been accumulated, the time and pathway for the first transition which will occur at the desired low temperature T_{low} can be determined and this transition is then accepted. This process is then repeated for a given desired interval of low-temperature time.

Our simulations were carried out using an embedded-atom method (EAM) potential [29] with a Cu substrate consisting of six (100) layers with width $L = 10 a$ (where a is the lattice constant of copper). The three bottom layers were held fixed while the temperature of the three top layers was controlled by a Langevin thermostat [30] with a friction coefficient of 10^{12} s^{-1} . In order to include the effects of strain, the substrate was compressed biaxially by 4% while periodic boundary conditions were assumed in the x - y (in-plane) directions. In order to simulate submonolayer growth, Cu atoms were deposited randomly with a deposition rate of 1 monolayer (ML)/sec while the substrate was equilibrated at 200 K. Since one monolayer corresponds to 200 atoms this implies a deposition rate of 200 atoms/sec or equivalently an average time interval between depositions of 0.005 sec. We note that while this deposition rate is still significantly faster than that used in experiments (typically 10^{-3} – 10^{-2} ML/sec) it is still

many orders of magnitude slower than is typically used in molecular dynamics simulations.

For each deposition, the Cu atoms were launched normally from a random position above the substrate at a height equal to that of the highest point of the film plus the cutoff distance $r_{\text{cut}} = 5.51 \text{ \AA}$ with an initial kinetic energy $K_i = 2 k_B T_m = 0.23 \text{ eV}$ (where k_B is the Boltzmann constant and $T_m = 1358 \text{ K}$ is the melting temperature of Cu). Molecular dynamics of the entire system was then carried out for 4 ps before continuing TAD simulations until the time for the next deposition event.

In order to maximize the acceleration or “boost” while minimizing the number of attempted high-temperature transitions, our TAD simulations were carried out with a high temperature $T_{\text{high}} = 650 \text{ K}$ [31]. The total number of atoms deposited in our simulations (27) corresponded to 0.135 ML, while the total time simulated (at 200 K) until the formation of a SF was approximately 0.14 sec. While TAD automatically calculates the activation barriers for all accepted events, for selected events we also calculated the corresponding forward and reverse prefactors (ν) using the Vineyard expression [32]

$\nu = \frac{\prod_{i=1}^{3N} \nu_i}{\prod_{i=1}^{3N-1} \nu_{s,i}}$, where ν_i ($\nu_{s,i}$) are the normal mode frequencies for the initial state (saddle point), respectively, and N is the number of moving atoms. In order to monitor the evolution of the free energy, including vibrational contributions, we have also calculated the change in free energy at $T = 200 \text{ K}$ with respect to a reference state with energy E_0 using the harmonic approximation expression $F = (E - E_0) + k_B T_{\text{low}} \ln \prod_{i=1}^{3N} \frac{\nu_i}{\nu_{0,i}}$, where E (E_0) and ν_i ($\nu_{0,i}$) are the minimized energy and normal mode frequencies of the selected (reference) state.

III. RESULTS

Figure 1 shows six of the key events which occur after the deposition of 0.135 ML and prior to the formation of a stacking fault at $t \simeq 0.14 \text{ sec}$. For each event, the initial, saddle, and final minimized configurations are shown along with the corresponding forward activation barriers. (The reverse activation barriers are shown in parentheses.) Also shown for both the states before and after each transition are the energy (E) and free energy (F) relative to the starting configuration in Fig. 1(a). As can be seen, due to the small system size as well as the relatively large rate of monomer diffusion (624 hops/sec) and dimer diffusion (8532 hops/sec) at 200 K, at this coverage there is only one island containing 25 atoms in the system, along with a dimer.

As indicated in Fig. 1(a), the first key event leading to the formation of a stacking fault corresponds to the pop-out of a Cu atom from the substrate, leading to the formation of a substrate vacancy. As indicated by the middle (saddle-point) configuration, this involves a collective move of two atoms, in which one atom leaves the substrate and attaches to the island at a kink site, while the second atom replaces the first atom, leaving a vacancy behind. We note that the barrier for vacancy formation in this case (0.63 eV) is significantly smaller than that for vacancy formation on the bare substrate away from the island (0.92 eV) or for vacancy formation at a straight island edge away from a kink (0.81 eV). In addition, the reverse

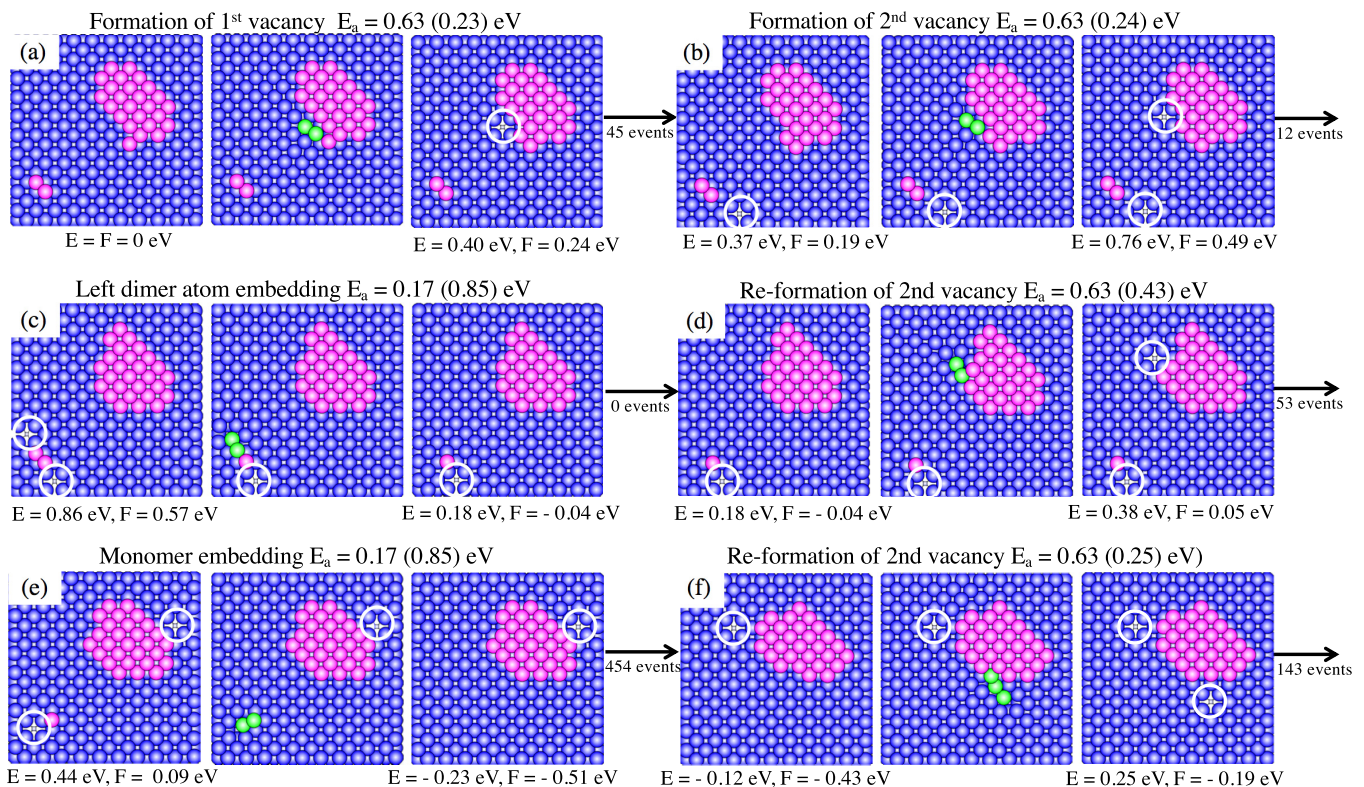


FIG. 1. Sequence of key events leading up to stacking fault formation. (a) Formation of first vacancy (b) Formation of second vacancy (c) Left dimer atom embedding and vacancy annihilation (d) Re-formation of second vacancy (e) Monomer embedding and vacancy annihilation (f) Re-formation of second vacancy.

barrier (0.23 eV) is higher than the barrier (0.13 eV) for the vacancy to diffuse away from the island, thus allowing the vacancy to diffuse away before it can be annihilated. As also shown in Fig. 1(a), while the energy increases significantly due to the increase in the number of missing nearest-neighbor bonds, the increase in the free energy is significantly smaller due to the increase in vibrational entropy.

Due to the relatively low diffusion barrier for vacancy diffusion, one would expect the vacancy to migrate rapidly via single hops away from the island. Instead, since the barriers for a variety of collective stringlike moves are comparable, while the corresponding prefactors are on the order of 100 times higher, after a few hops back and forth near the island edge, the vacancy then moves by a sequence of three long-distance stringlike moves [29] involving 4–6 substrate atoms, until it is near the dimer as shown in Fig. 1(b). A variety of additional long-distance vacancy diffusion moves are then carried out along with a number of island rearrangements after which the island returns to its initial state.

As shown in Fig. 1(b), a second vacancy is then formed near an island kink site with the same activation energy as for the first. A variety of low-barrier collective vacancy diffusion moves then occur, including a seven-atom move which includes both the island and substrate, after which both vacancies are near the dimer as shown by the first picture in Fig. 1(c). This leads to the very low activation barrier vacancy annihilation event shown in Fig. 1(c) in which the left dimer atom pushes a nearby substrate atom into the vacancy and replaces it. While the free energy at this point is slightly lower

than that of the initial state, immediately after embedding the free energy is again increased by the re-formation of a second vacancy at a kink site, as shown in Fig. 1(d). Even though the activation barriers are the same, as discussed in more detail below, the energy increase for this event is almost 0.2 eV smaller than for the vacancy formation event shown in Fig. 1(b).

Figures 1(e) and 1(f) show the two key remaining transitions leading up to the stacking fault transition shown in Fig. 2. In particular, Fig. 1(e) shows the embedding of the remaining monomer via an exchange process which involves a nearby substrate atom and one of the two substrate vacancies. The barrier for this process (0.17 eV) is equal to that for the first embedding process, while the resulting free energy is now significantly lower than that for the initial state. This is then followed by a large number (454) of low-barrier collective vacancy diffusion processes as well as some island rearrangement, leading to the initial configuration shown in Fig. 1(f). A second substrate vacancy is then re-formed near an island kink site via a collective three-atom pop-out event with the same barrier (0.63 eV) as for the other two vacancy formation events. As can be seen, the system now consists of two substrate vacancies and one island containing 27 atoms, while the free energy remains negative with respect to the configuration shown in Fig. 1(a).

While a total of 570 events take place during the time from the first configuration in Fig. 1(a) to the final configuration in Fig. 1(f)—due to the relatively low barriers of these events—this corresponds to a time difference of only 1.3 msec. A

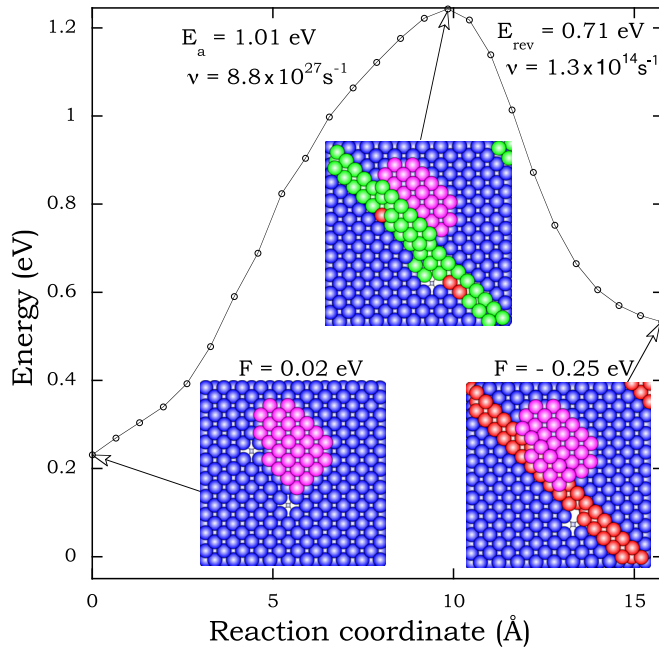


FIG. 2. Nudged elastic band results for stacking fault formation transition. Top picture indicates saddle-point configuration while the bottom two pictures correspond to initial and final minimized configurations.

comparison of the island configurations indicates that while the vacancy formation transitions in Fig. 1(b) and Fig. 1(f) correspond to the creation of two additional first-, second-, and third-neighbor “bonds” in the island, for the transition shown in Fig. 1(d) only one additional second-neighbor bond is created. This leads to a reduction in the total strain energy and explains the reduced increase in the total energy for the vacancy formation event in Fig. 1(d) compared to those shown in Figs. 1(b) and 1(f).

As shown in Fig. 2, after 143 additional low-barrier events (including primarily vacancy diffusion events and some island rearrangement) a collective move involving 69 atoms occurs, leading to the formation of a stacking fault. We note that the activation barrier for this event is extremely large (1.01 eV) which implies that with a normal prefactor of the order of 10^{13} s^{-1} it would take a time of the order of 10^{12} sec before occurring. However, the Vineyard prefactor for this event is also extremely large ($\nu = 8.8 \times 10^{27} \text{ s}^{-1}$). This implies an average waiting time at 200 K of only 3 msec, which is somewhat larger than but still consistent with the elapsed low-temperature time of approximately 1.5 msec. As indicated in Fig. 2 the reverse prefactor is significantly smaller, and as a result the reverse transition rate is negligible at 200 K.

Examination of the normal modes also indicates that the extremely large forward prefactor is primarily due to the presence of a large number of vibrational modes at the saddle point whose frequencies are slightly lower than for the initial state. Similarly, the much smaller reverse prefactor is due to the presence of a large number of low-frequency modes in the final stacking fault state. These results indicate that both the transition state and the final SF state have much higher vibrational entropy than the initial state. This is consistent

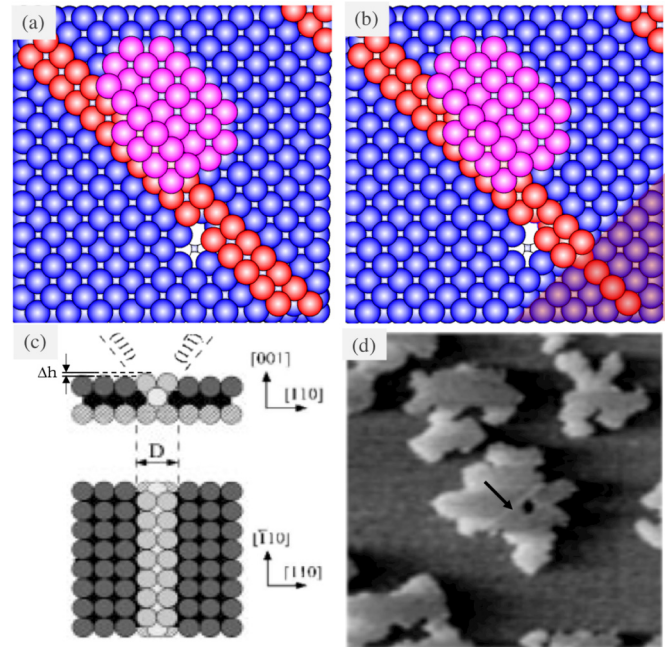


FIG. 3. (a) Closeup of final configuration shown in Fig. 2(b). Same as (a) but with top substrate layer atoms removed in the bottom right-hand corner. Stacking fault atoms in the row below the substrate layer are shown in red, while remaining atoms are purple. (c) Faceting model for Cu/Ni(100) [9] (d) STM picture (from Ref. [7]) showing single-Cu islands grown on Ni(100) at 350 K after 0.35 ML have been deposited. Arrow points to single-row stripe in center island.

with the fact that even though the energy of the stacking fault state is 0.3 eV higher than that of the initial state, the total relative free energy at 200 K (-0.25 eV) is reduced by 0.27 eV. We have also carried out TAD annealing simulations at 200 K in order to test the stability of the stacking fault configuration. As expected, for the maximum annealing time studied (1.1 sec) the stacking fault remains stable.

Figure 3(a) shows a closeup of the stacking fault (SF) configuration which includes two rows of the top substrate layer as well as two rows of the island, each of which have shifted by one half the nearest-neighbor distance. As can be seen, there is still a vacancy in the substrate next to the stacking fault as well as a partial vacancy in the stacking fault itself. Figure 3(b) shows a view of the same configuration in which the top substrate layer in the bottom right corner of the system has been removed (see caption). As can also be seen, one row of atoms in the layer below the substrate has also shifted by one half the nearest-neighbor distance, thus indicating the formation of small (111) facets along the stacking fault defect.

For comparison, the suggested structure [6] for the formation of stripe defects in Cu/Ni(100) growth after 3 ML have been deposited at 350 K is also shown in Fig. 3(c). As can be seen, except for the difference in the number of layers, the two structures are essentially identical. In addition, an analysis of the configuration in Fig. 3(b) indicates that for the minimized (0 K) state, the atoms in the surface stripe (stripe below the surface) have also shifted up by an amount $\Delta h = 0.35 \text{ \AA}$ (0.33 \AA) from their initial positions. Due to the presence of

relaxation, this amount is close to but somewhat smaller than the prediction ($\Delta h \simeq 0.4 \text{ \AA}$) based on a “hard-sphere model” which takes into account the difference in geometry between a fourfold hollow site and a bridge site. We note that the experimentally measured value [7] obtained for single-row stripes formed in second-layer Cu/Ni(100) islands at 350 K ($\Delta h = 0.5 \pm 0.15 \text{ \AA}$) is slightly higher than this value, perhaps due in part to the effects of thermal expansion. For comparison, also shown in Fig. 3(d) is an STM picture which indicates a single-row stripe SF in one of the Cu islands grown on Ni(100) at 350 K after only 0.35 ML have been deposited.

IV. DISCUSSION

In order to understand the effects of strain on defect formation in the early stages of heteroepitaxial growth, as well as to separate out chemical effects from strain effects, we have carried out temperature-accelerated dynamics simulations of the growth of Cu on a strained Cu(100) substrate at $T = 200 \text{ K}$, with a deposition rate (1 ML/s) close to typical experimental values. Since our simulation temperature is somewhat lower than typical experimental temperatures ($T \geq 300 \text{ K}$), in order to observe defect formation on the time scale of our simulations, our simulations were carried using a somewhat larger value of compressive strain than that in Cu/Ni (100) growth.

Our results indicate that, in addition to compressive strain, the formation of both islands and vacancies is crucial to stacking fault formation. In particular, we find that when two substrate vacancies have formed and have reached the right configuration near an island, a stacking fault is formed. Interestingly, while the activation barrier for this many-atom collective event is extremely large (1.0 eV), the prefactor is also “gigantic” (e.g., $8.8 \times 10^{27} \text{ s}^{-1}$), and as a result the average time interval for this transition is only approximately 3.2 msec. The large prefactor is due to the presence of a large number of vibrational modes at the saddle point whose frequencies are slightly lower than for the initial state. Similarly, the much smaller reverse prefactor is also due to the presence of a large number of low-frequency modes in the final stacking fault state. As a result, even though the energy is higher, the free energy of the stacking fault state is lower than that of the initial state. We note that in previous work on the transformation of 20–45 atom vacancy voids to stacking fault tetrahedra in unstrained bulk Cu, a very large prefactor with a correspondingly large energy barrier and number of atoms involved in the transition has also been observed due to entropic effects [33].

Our results also indicate that the presence of islands is crucial for the formation of vacancies. In particular, while the presence of compressive strain lowers the energy for vacancy formation in the bare substrate from 1.54 eV to 1.32 eV, this still leads to a negligible equilibrium vacancy density. Similarly, at 200 K, the difference in free energy of a vacancy-monomer pair and that of the bare substrate is approximately 1.27 eV. In contrast, in the presence of compressive strain the formation energy of a vacancy at an island kink site is significantly lower (ranging from 0.2 eV to 0.4 eV depending on the kink site) while the free energy increases by only

0.1–0.3 eV depending on the island configuration. Thus, island formation and growth play a crucial role in promoting vacancy formation.

In addition to these results, a number of other interesting effects have been observed in our simulations. In particular, we found that—rather than migrating via single-atom hops—since the barriers for collective moves are comparable in the presence of compressive strain while the prefactors are on the order of 100 times higher, substrate vacancies diffuse primarily via collective (3–6 atom) string-like moves. In contrast, in the absence of strain the barriers for vacancy diffusion are significantly higher ranging from 0.44 eV for single-atom moves to 0.6–1.0 eV for stringlike moves. We also found that while the value of the barrier for monomer diffusion is significantly reduced (from 0.51 eV to 0.42 eV) in the presence of strain, the key barrier for dimer diffusion (for which the corresponding transition involves one atom of the dimer hopping from a nearest-neighbor site of the other dimer atom to that atom’s next-nearest neighbor site) is also significantly reduced (from 0.49 eV to 0.38 eV). Interestingly, the next-nearest neighbor dimer separation was also found to be significantly reduced in the presence of strain (2.72 Å with strain versus 3.3 Å without strain) even though the nearest-neighbor separation (2.47–2.49 Å) is almost the same with and without strain.

Finally, it is interesting to compare our simulation results with those obtained experimentally for Cu/Ni(100) growth at 350 K. While there is no compressive strain in the substrate in this case, there is a 2.7% compressive strain in the islands. As a result, the initial (single row) stripes occur in the islands [see Fig. 3(d)] rather than the substrate-plus-island as in our simulations. In addition, the formation of multilayer SFs only occurs after the deposition of more than one layer.

Since our results indicate that vacancies play an important role in the formation of SFs during the growth of Cu on strained Cu(100), we conjecture that this is also the case in Cu/Ni(100) growth. As already discussed in the Introduction, it has been previously shown [20] that for Cu/Ni(100) growth, the barrier for in-plane pop-out events at island edges with kinks decreases significantly with island size. While these events have already been demonstrated [20] to lead to the ramified island shapes observed experimentally, they can also lead to vacancy formation within the island. Accordingly, we speculate that one possible pathway for SF formation in Cu/Ni(100) submonolayer islands might involve the simultaneous formation of two or more vacancies in an island, perhaps due to in-plane pop-out events, since such events are kinetically favorable for sufficiently large islands and/or temperatures. It would be of interest to carry out simulations of Cu islands on Ni(100) for larger island sizes and higher temperatures to see if this is the case.

ACKNOWLEDGMENTS

This work was supported in part by NSF Grant No. DMR-1410840. The authors also gratefully acknowledge funding support from the US Air Force Research Laboratory, Space Vehicles Directorate, under Contract No. FA9453-19-C-1002. We would also like to acknowledge a grant of computer time from the Ohio Supercomputer Center.

- [1] R. J. Asaro and W. A. Tiller, *Metal. Trans.* **3**, 1789 (1972).
- [2] M. A. Grinfeld, *Sov. Phys. Doklady* **31**, 831 (1986).
- [3] C. Humphreys, D. Maher, D. Eaglesham, E. Kvam, and I. Salisbury, *J. Phys. III (France)* **1**, 1119 (1991).
- [4] Y.-W. Mo, D. E. Savage, B. S. Swartzentruber, and M. G. Lagally, *Phys. Rev. Lett.* **65**, 1020 (1990).
- [5] J. Tersoff and R. M. Tromp, *Phys. Rev. Lett.* **70**, 2782 (1993).
- [6] B. Müller, L. Nedelmann, B. Fischer, A. Fricke, and K. Kern, *J. Vac. Sci. Technol. A* **14**, 1878 (1996).
- [7] B. Müller, B. Fischer, L. Nedelmann, A. Fricke, and K. Kern, *Phys. Rev. Lett.* **76**, 2358 (1996).
- [8] B. Müller, L. P. Nedelmann, B. Fischer, H. Brune, J. V. Barth, and K. Kern, *Phys. Rev. Lett.* **80**, 2642 (1998).
- [9] B. Müller, L. Nedelmann, B. Fischer, H. Brune, J. V. Barth, and K. Kern, D. Erdös, and J. Wollschläger, *Surf. Rev. Lett.* **5**, 769 (1998); **8**, 169 (2001).
- [10] S. H. Brongersma, M. R. Castell, D. D. Perovic, and M. Zinke-Allmang, *Phys. Rev. Lett.* **80**, 3795 (1998).
- [11] J. Hrbek and R. Q. Hwang, *Curr. Opin. Solid State Mater. Sci.* **5**, 67 (2001).
- [12] W. Ma, R. Nötzel, H.-P. Schöhherr, and K. H. Ploog, *Appl. Phys. Lett.* **79**, 4219 (2001).
- [13] V. Fournée, J. Ledieu, T. Cai, and P. A. Thiel, *Phys. Rev. B* **67**, 155401 (2003).
- [14] N. V. Medhekar, V. B. Shenoy, J. B. Hannon, and R. M. Tromp, *Phys. Rev. Lett.* **99**, 156102 (2007).
- [15] M. S. J. Marshall and M. R. Castell, *Phys. Rev. Lett.* **102**, 146102 (2009).
- [16] Y. Li, M. Liu, D. Ma, D. Yu, X. Chen, X.-C. Ma, Q.-K. Xue, K. Xu, J.-F. Jia, and F. Liu, *Phys. Rev. Lett.* **103**, 076102 (2009).
- [17] K. Liu, I. Berbezier, T. David, L. Favre, A. Ronda, M. Abbarchi, P. Voorhees, and J.-N. Aqua, *Phys. Rev. Materials* **1**, 053402 (2017).
- [18] J. de la Figuera, K. F. McCarty, and N. C. Bartelt, *Surf. Sci.* **682**, 43 (2019).
- [19] A. Li, F. Liu, and M. G. Lagally, *Phys. Rev. Lett.* **85**, 1922 (2000).
- [20] Y. Shim and J. G. Amar, *Phys. Rev. Lett.* **108**, 076102 (2012).
- [21] Z. Chen, J. Zhang, S. Xu, J. Xue, T. Jiang, and Y. Hao, *Mater. Res. Bull.* **89**, 193 (2017).
- [22] X. Feng, J. U. Surjadi, X. Li, and Y. Lu, *J. Alloys Compd.* **844**, 156187 (2020).
- [23] Y. Shim and J. G. Amar, *J. Chem. Phys.* **145**, 014105 (2016).
- [24] The choice of this value was also motivated by preliminary calculations in which we found that the barrier for vacancy diffusion in a Cu monolayer on a Ni(100) substrate decreases linearly with increasing compressive strain and then abruptly goes to zero at a strain value of 4.7%.
- [25] M. R. Sørensen and A. F. Voter, *J. Chem. Phys.* **112**, 9599 (2000).
- [26] D. Perez, B. P. Uberuaga, Y. Shim, J. G. Amar, and A. F. Voter, *Annu. Rep. Comput. Chem.* **5**, 79 (2009).
- [27] R. J. Zamora, B. P. Uberuaga, D. Perez, and A. F. Voter, *Annu. Rev. Chem. Biomol. Eng.* **7**, 87 (2016).
- [28] G. Henkelman, *Annu. Rev. Mater. Res.* **47**, 199 (2017).
- [29] Y. Mishin, M. J. Mehl, D. A. Papaconstantopoulos, A. F. Voter, and J. D. Kress, *Phys. Rev. B* **63**, 224106 (2001).
- [30] M. P. Allen and D. J. Tildesley, *Computer Simulations of Liquids* (Oxford, New York, 1987), p. 263.
- [31] In our TAD simulations a minimum value of the prefactor $v_{\min} = 10^{12}/s$ was also assumed along with an uncertainty $\delta = 0.1$.
- [32] G. Vineyard, *J. Phys. Chem. Solids* **3**, 121 (1957).
- [33] B. P. Uberuaga, R. G. Hoagland, A. F. Voter, and S. M. Valone, *Phys. Rev. Lett.* **99**, 135501 (2007).